

Biomembrane-Modified Field Effect Transistors for Sensitive and Quantitative Detection of Biological Toxins and Pathogens

Hua Gong,^{†,‡} Fang Chen,^{†,‡} Zhenlong Huang,^{†,‡} Yue Gu,^{†,‡} Qiangzhe Zhang,[†] Yijie Chen,[†] Yue Zhang,[†] Jia Zhuang,[†] Yoon-Kyoung Cho,^{‡,§} Ronnie H. Fang,[†] Weiwei Gao,[†] Sheng Xu,^{*,†} and Liangfang Zhang^{*,†}

[†]Department of Nanoengineering, University of California San Diego, La Jolla, California 92093, United States

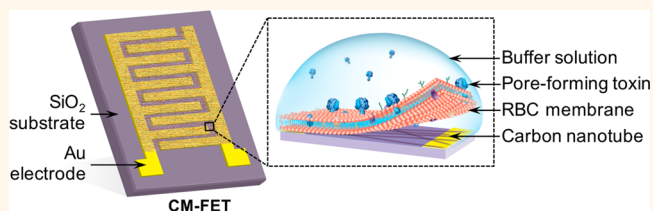
[‡]Center for Soft and Living Matter, Institute for Basic Science (IBS), Ulsan, 44919, Republic of Korea

[§]Department of Biomedical Engineering, Ulsan National Institute of Science and Technology (UNIST), Ulsan, 44919, Republic of Korea

Supporting Information

ABSTRACT: The efforts of detecting bioactive targets with complex, dynamic, and unknown molecular profiles have inspired the development of various biosensor platforms. Herein, we report a cell-membrane-modified field effect transistor (FET) as a function-based nanosensor for the detection and quantitative measurement of numerous toxins and biological samples. By coating carbon nanotube FETs with natural red blood cell membranes, the resulting biomimetic nanosensor can selectively interact with and absorb broad-spectrum hemolytic toxins regardless of their molecular structures. Toxin–biomembrane interactions alter the local charge distribution at the FET surface in an ultrasensitive and concentration-dependent manner, resulting in a detection limit down to the femtomolar (fM) range. Accurate and quantitative measurements are enabled *via* a built-in calibration mechanism of the sensor, which overcomes batch-to-batch fabrication variations, and are demonstrated using three distinct toxins and various complex bacterial supernatants. The measured signals of bacterium-secreted proteins correlate linearly with the actual bacterial numbers, making the biosensor a nontraditional approach to rapidly detecting bacterial concentrations without a need to count bacterial colonies.

KEYWORDS: biosensor, cell membrane, field effect transistor, carbon nanotube, hemolysis



The development of nanoscale biosensors has gained significant interest in the past few decades, leading to a variety of fast and reliable platforms for the detection of pathogens, toxins, and bioactive compounds.^{1–4} Their applications are ever-growing, ranging from clinical and pharmaceutical analyses to environment and biodefense-related detections.^{5–8} Development of the next-generation biosensors increasingly seeks the capability of detecting bioactive targets with complex and dynamic molecular profiles, often unknown, in a highly sensitive, label-free, and broad-spectrum fashion.^{9–12} Conventional approaches relying primarily on molecular structures or chemical characteristics of the targets for recognition are only effective for specific predefined targets and are therefore unable to meet the above challenge.^{13,14} In this perspective, function-based detection systems capable of reporting the presence of biological substances or threat agents in a physiologically relevant manner but without prior knowledge of the targets are highly desirable. Herein, we report the design and characterization of

a function-based nanosensor that combines a carbon nanotube field effect transistor (FET) with natural cell membranes (Figure 1a). The cell-membrane-functionalized FET (denoted “CM-FET”) nanosensor can detect the pore-forming activities of a wide spectrum of biological toxins in a rapid, ultrasensitive, and quantitative manner.

The use of natural cell membranes to coat synthetic nanomaterials has recently emerged as a versatile top-down method for material functionalization.^{15–17} In particular, the membrane of red blood cells (RBCs) has become an attractive coating material that absorbs and neutralizes numerous pore-forming toxins (PFTs) despite the enormous structural diversity of these toxins.¹⁸ This is achieved by leveraging the fact that, regardless of their specific mode of action, these

Received: January 31, 2019

Accepted: March 4, 2019

Published: March 4, 2019

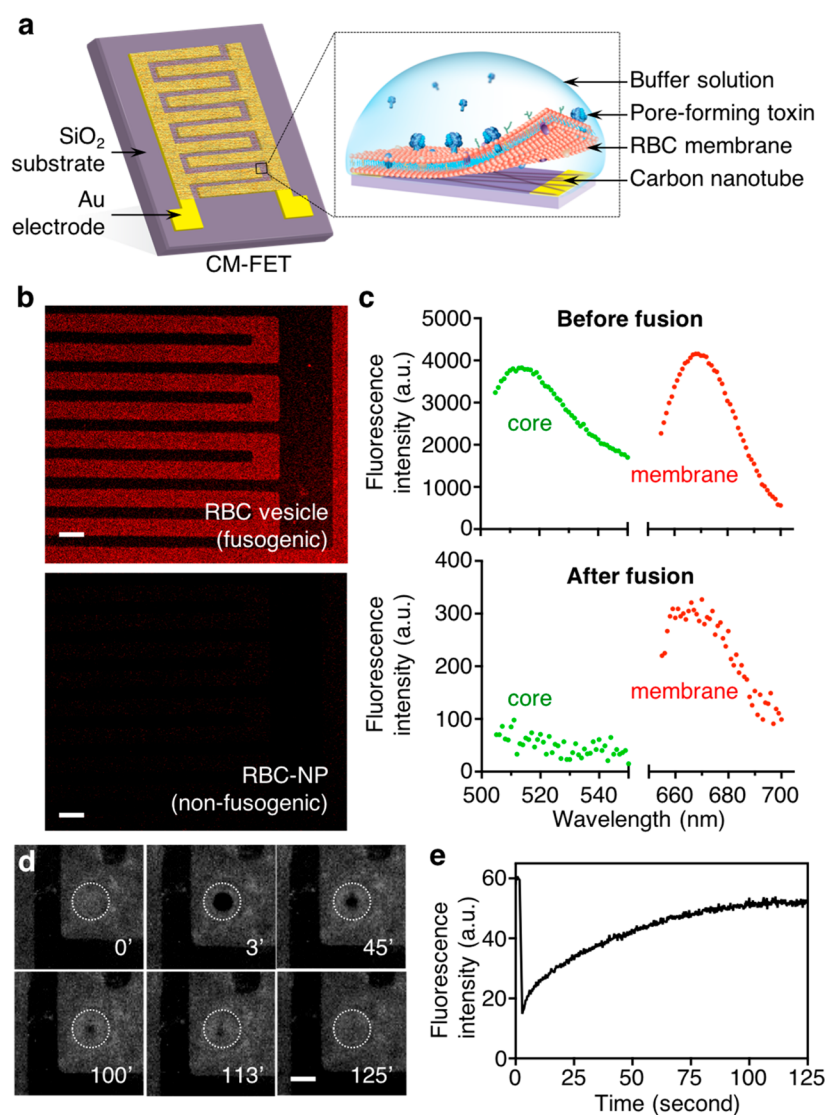


Figure 1. Fabrication and characterization of cell-membrane-coated carbon nanotube field effect transistors (CM-FETs). (a) Schematic construct of a CM-FET consisting of RBC membranes coated on the FET surface. (b) (Top panel) Fusogenic RBC vesicles labeled with DiD dye were incubated with the FET substrate, and the fluorescence image was taken after removal of excessive vesicles (scale bar = 100 μm). (Bottom panel) Nonfusogenic RBC membrane-coated nanoparticles (RBC-NPs) were tested in parallel as a control (scale bar = 100 μm). (c) RBC vesicles were labeled with two distinct fluorescent dyes: DiD (red) in the cell membrane and calcein-AM (green) in the aqueous compartment of the vesicles. Fluorescence emission spectra of the RBC vesicles before (top) and after (bottom) their incubation with the FET substrate were taken and compared. (d) Fluorescence-recovery-after-photobleaching (FRAP) study of RBC membranes coated on the FET substrate (scale bar = 50 μm). (E) Fluorescence intensity recovery of regions of interest after photobleaching. The diffusion coefficient was determined to be 0.38 $\mu\text{m}^2 \text{S}^{-1}$.

toxins must in one way or another interact directly with the cell membranes.¹⁹ In this design, the semiconductive carbon-nanotube-based FET is coated with RBC membranes. The RBC membranes will interact selectively with PFTs that have membrane lytic activities, regardless of the PFT structural specificity. The binding event between the membranes and the target toxins disturbs the electrical double layer within proximity of the carbon nanotubes, which in turn changes the conductance of the FET.^{20,21} Compared to synthetic lipid-bilayer-based biosensors, CM-FETs replicate natural interactions between cell membranes and targets without the requirement to optimize the membrane composition or experimental conditions.²² Compared to cell-based biosensors that use living cells for detection, CM-FETs eliminate the necessity of cell culture and maintenance while preserving

biofunction-driven, broad-spectrum, and high-content detection capabilities with superior stability and selectivity.²³

RESULTS AND DISCUSSION

Fabrication and Characterization of CM-FET. The fabrication of the CM-FET was divided into two steps. In the first step, semiconductive single-walled carbon nanotubes (SWCNTs) were spray-coated onto an oxidized silicon substrate with patterned interdigitated electrodes. Sprayed SWCNTs formed meshes on the silica surface bridging the adjacent electrodes and rendering the device semiconductive (Figure S1). In the second step, purified RBC membranes were sonicated to generate RBC vesicles with an average diameter of about 120 nm, followed by drop casting onto the device surface, where the small vesicles fused onto the flat substrate

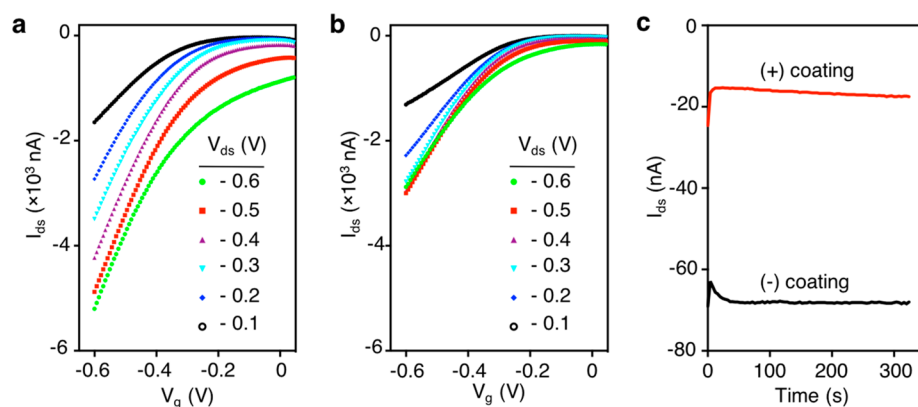


Figure 2. Semiconductive properties of CM-FETs. (a) I_{ds} - V_g curves of uncoated FETs with the V_{ds} ranging from -0.6 V to -0.1 V. (b) I_{ds} - V_g curves of FETs after cell membrane coating with the V_{ds} ranging from -0.6 V to -0.1 V. (c) I_{ds} -time curve of uncoated FETs and FETs with cell membrane coating ($V_{ds} = -0.3$ V, $V_g = 0$ V).

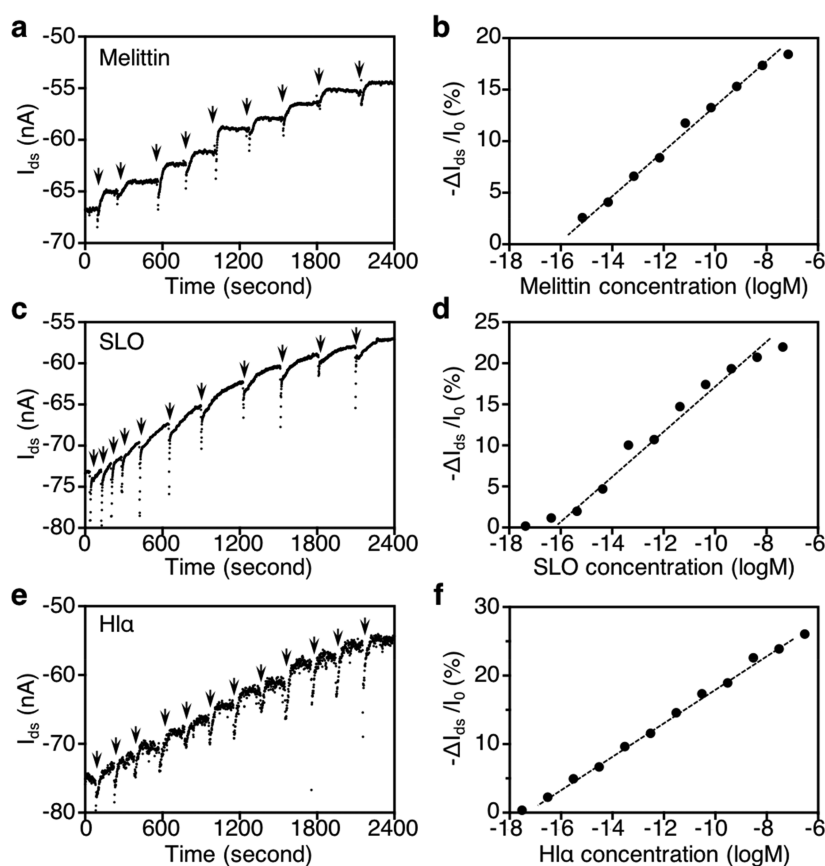


Figure 3. Functional test of CM-FETs using distinct pore-forming toxins (PFTs): (a, b) melittin, (c, d) streptolysin O, and (e, f) Hla. For each type of toxin, CM-FETs were used to measure the channel conductance as a function of time and toxin concentrations. Typical I_{ds} -time curves of each toxin (a, c, e) were measured, and values of I_{ds} change relative to the basal level ($\Delta I_{ds}/I_0$) were plotted against toxin concentrations (b, d, f).

surfaces to form a uniform bilayer membrane coating. To verify vesicle fusion on the device, RBC vesicles were labeled with a lipophilic dye (1'-dioctadecyl-3,3',3'-tetramethylindodicarbocyanine, 4-chlorobenzenesulfonate salt, DiD, excitation/emission = 644/665 nm) and then incubated with the device for 1 h. The excessive vesicles were removed by repeated washing. Following the fabrication, the fluorescence image of the device shows a strong signal from the labeled membranes with even distribution on the oxide surface, which indicates uniform coating of the membrane bilayer (Figure 1b). The

dark regions match the pattern of the interdigitated gold electrodes that quench the fluorescence of the dye. To verify that such membrane retention on the device was indeed due to the vesicle fusion instead of nonspecific adsorption, we prepared nonfusogenic RBC vesicles by precoating the membranes onto polymeric nanoparticles (RBC-NPs). After wrapping around solid cores, these vesicles formed a stable membrane-core interface and therefore could not fuse with the electrode substrate.²⁴ After applying the same incubation and washing steps, little fluorescence was detected from the

treated device surface, therefore confirming the role of vesicle–substrate fusion in retaining the cell membranes.

To further validate the fusion process, we prepared dual-fluorescence-labeled RBC vesicles: one fluorescence dye (DiD) was incorporated into the bilayer membrane of the vesicles and the other (calcein, excitation/emission = 495/515 nm) encapsulated inside the aqueous compartment of the vesicles. Following the same incubation process, however, only the fluorescence signal from the membrane was detected from the device surface, indicating the loss of inner content during the vesicle–substrate fusion process (Figure 1c). Additionally, we performed a fluorescence recovery after photobleaching (FRAP) study to measure the lateral diffusion coefficient of the membrane lipids after they are coated onto the FET. In the study, fluorescence dye DiD was doped into the cell membrane, and an incident laser beam at a wavelength of 633 nm was used to photobleach a spot (spot radius 6.57 μm , Figure 1d). Upon removal of the laser, fluorescence in the bleached area recovered gradually, and full recovery was observed after approximately 125 s. From the recovery curve (Figure 1e), the translational diffusion coefficient of the membrane lipids on CM-FET was calculated to be $0.38 \mu\text{m}^2 \text{S}^{-1}$ based on a supported lipid bilayer model of $D = 0.88r^2/(4t_{1/2})$ (D : translational diffusion coefficient; r : radius of photobleaching area; and $t_{1/2}$: time needed to recover half of its maximum fluorescence).²⁵ This value is comparable to that of the lipids in intact RBCs ($D = 0.82 \mu\text{m}^2 \text{s}^{-1}$), further implying a two-dimensional planar membrane layer on the CM-FET.^{26,27}

The electrical property of CM-FETs was also tested (Figure 2a,b). For each fixed drain–source voltage (V_{ds}), the absolute value of drain–source current (I_{ds}) increased from “off” state ($I_{\text{ds}} = 0$) to “on” state ($I_{\text{ds}} > 0$) as the gate voltage (V_{g}) became more negative, suggesting that the CM-FET maintains p-type semiconductive characteristics after the membrane coating.²⁸ It was found that at the same V_{g} and V_{ds} values, the absolute current (I_{ds}) of the CM-FET was much smaller than that of an uncoated FET, suggesting increased resistance upon cell membrane coating. Figure 2c shows the I_{ds} –time curves of an uncoated FET and CM-FET at $V_{\text{ds}} = -0.3 \text{ V}$ and $V_{\text{g}} = 0 \text{ V}$. The absolute value of I_{ds} decreased significantly upon membrane coating. This further confirms the coating of an RBC membrane onto the FET surface, consistent with the above characterization of membrane coating (Figure 1b,c).

Detection of Broad-Spectrum Hemolytic Toxins. We first tested the ability of CM-FETs to detect PFTs. In the study, three distinct model PFTs were selected including melittin ($M_{\text{w}} = 2.8 \text{ kDa}$), streptolysin O (SLO, $M_{\text{w}} = 69 \text{ kDa}$), and alpha hemolysin (Hl α , $M_{\text{w}} = 33 \text{ kDa}$). For each type of toxin, we used CM-FETs to measure the channel conductance as a function of time and toxin concentrations. Prior to the addition of toxin solutions to the device, solutions of dithiothreitol and bovine serum albumin were added to block possible nonspecific binding (Figure S2). We first tested the detection limits (*i.e.*, the lowest toxin concentration that induces a perceptible conductance change). In the study, CM-FETs responded to melittin, SLO, and Hl α at concentrations no less than 0.7, 0.04, and 0.03 fM, respectively (corresponding to 4.8, 2.8, and 0.99 ng L^{-1} , respectively). The detection limit of sub-fM range is substantially lower than the currently available whole-cell-based hemolytic assay (nM range), ELISA assay (pM range), and chemically modified nanowire-based FETs (nM range).^{18,29,30} The CM-FET channel conductance

decreased stepwisely with discrete changes of toxin concentration. These results are attributable to toxin molecules that decrease the conductance by attracting holes in p-type CM-FETs.^{31,32} The devices remained responsive to toxin concentrations in the range of fM to μM (Figure 3a,c,e). A typical plot of the conductance–logarithmic toxin concentration relationship is linear over 0.7 fM to 70 nM for melittin, 0.04 fM to 42.8 nM for SLO, and 0.03 fM to 300 nM for Hl α , respectively (Figure 3b,d,f). The linear response is likely attributed to an approximately linear change in the total surface charge density *versus* logarithmic toxin concentration.³⁰ The response of CM-FETs to toxin solutions with good linearity over a wide concentration range suggests that the device can be used as an ultrasensitive and high-content biosensor to quantitatively detect toxins.

Detection of Bacterial Whole Secreted Proteins. Linear CM-FET responses given by various types of PFTs motivated us to apply the CM-FETs to detect and quantify the overall pore-forming activities of live bacterial culture, a complex biological solution known to contain a vast mixture of hemolytic toxins. The feasibility of this concept was demonstrated using the culture of methicillin-resistant *Staphylococcus aureus* (MRSA), which contains multiple well-characterized PFTs secreted by the bacteria.³³ A grand challenge of using FET-based biosensors to detect and quantify the pore-forming activity of complex biological fluids is the lack of a known calibration curve. The batch variations of FET sensors, including the CM-FETs, render any external reference curves irrelevant. To overcome this intrinsic technical barrier, we included a series of Hl α solutions with well-defined concentrations as an internal reference to calibrate each CM-FET for quantitative measurements of the hemolytic activity of complex biological samples. Detailed procedures are summarized in Supporting Information Table S1.

In the study, we selected various MRSA bacterial culture supernatants for measurements (Table S2). First, Hl α and MRSA culture supernatant samples of different dilutions were added alternately onto the CM-FET, and the device I_{ds} was measured as a function of time (Figure 4a). Three MRSA culture samples obtained from either different incubation times or different batches, together with the Hl α reference samples, were measured with nine different devices (three distinct devices for each sample) (Figure S3, and Table S3). Following the measurement, the response $\Delta I_{\text{ds}}/I_0$ values corresponding to the Hl α reference and MRSA supernatant were plotted against their dilution factors, respectively, generating nine pairs of linear curves that corresponded to the Hl α concentrations and supernatant dilution factors (Figure 4b). On the same device, the fitted lines for the Hl α and supernatant samples are parallel, suggesting that the membrane-active components in the MRSA supernatant share a similar concentration-dependence to the Hl α reference in inducing signal changes on the CM-FETs (Table S4). Indeed, comparing the slopes of the Hl α references and the supernatant samples with the F test showed no statistical significance ($p > 0.05$, Table S5). Since the actual concentration of supernatant in terms of hemolytic toxins is unknown but the concentration of Hl α as an internal reference is well-defined, the distance between the X -intercepts of the two parallel linear curves (denoted ΔX) will thus be able to quantitatively describe the hemolytic activity of a given MRSA supernatant as an equivalence of the hemolytic activity of the corresponding Hl α concentration. The ΔX value implies relative potency of a sample in interacting with the RBC

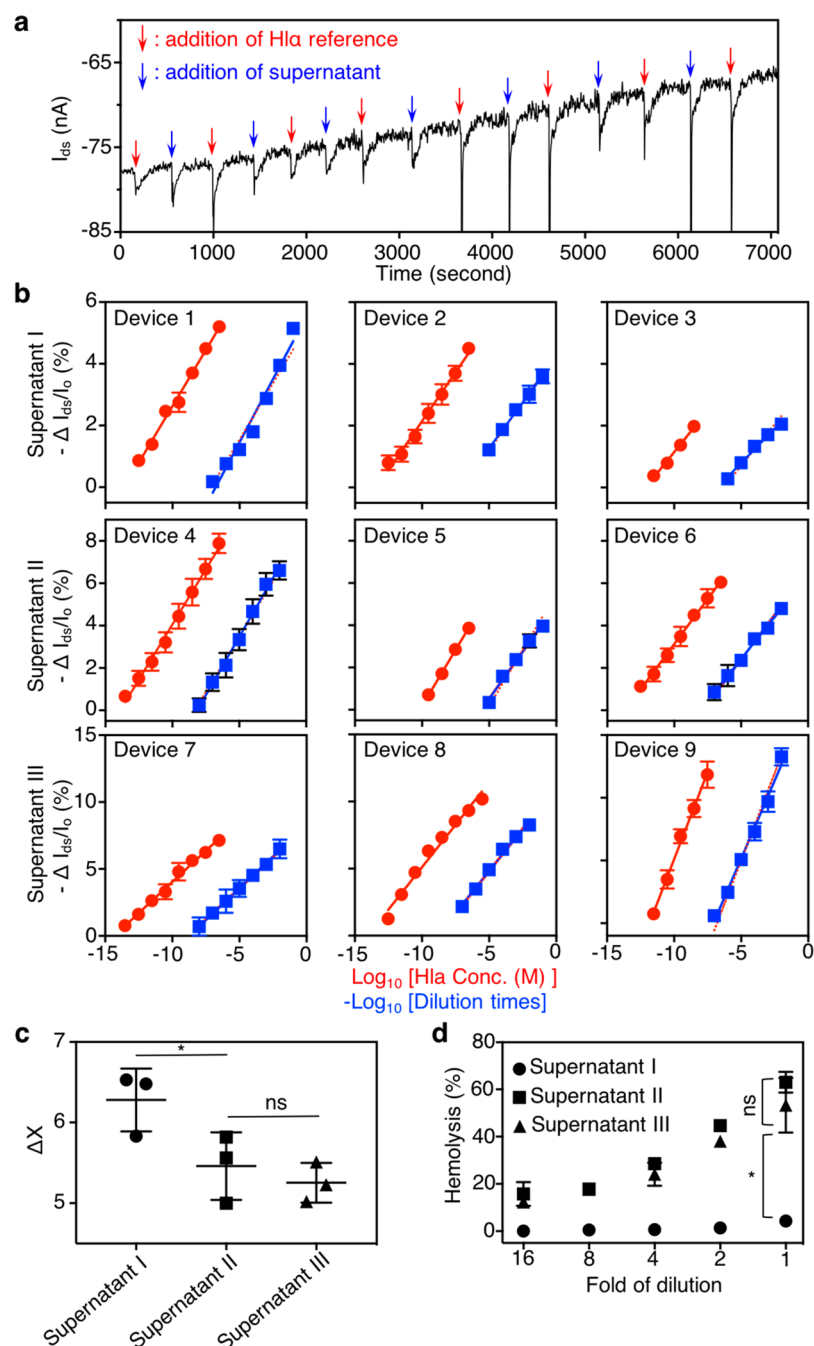


Figure 4. Quantitative detection and measurement of the hemolytic activity of complex biological fluids with CM-FET. Measurements were carried out with MRSA bacterial culture supernatants as a model system and Hla as an internal reference. The I_{ds} change of CM-FETs was measured after alternately adding Hla and MRSA supernatant. Both Hla and the supernatant were 10-fold serially diluted into different concentrations. (a) Representative I_{ds} -time curves after alternately adding Hla and MRSA supernatant from low to high concentrations. (b) Changes in I_{ds} for the Hla and MRSA supernatant relative to the initial current I_0 ($\Delta I_{ds}/I_0\%$) were extracted separately from the I_{ds} -time curve in (a) and plotted against the dilution factors of the supernatant. Linear fitting of the two curves was applied first (red solid line for Hla reference; blue solid line for MRSA supernatant). Then the supernatant sample was fitted linearly with a slope equal to that of the Hla (red dashed line). (c) The distance (ΔX) between the linear fitting of the Hla curve (solid red line) and linear fitting of the supernatant curve with the same slope of the Hla was calculated for each device in (b). The ΔX values are used to correlate the measured hemolytic activity of the supernatant to that of Hla. (d) To validate the accuracy of such correlation obtained in (c), the actual hemolytic activity of the three MRSA supernatants was directly measured using a conventional cell-based hemolytic assay.

membranes and can be compared between different samples and measurements. In the study, the ΔX measured from supernatant I is significantly higher when compared with those from supernatant samples II and III, while the ΔX values measured from the supernatants II and III show no statistical

significance (Figure 4c). This indicates that supernatant I is less hemolytic than supernatants II and III because it is equivalent to a much lower Hla concentration. To further validate the hemolytic activity measured by the CM-FETs, we tested the hemolytic activity of undiluted supernatant samples

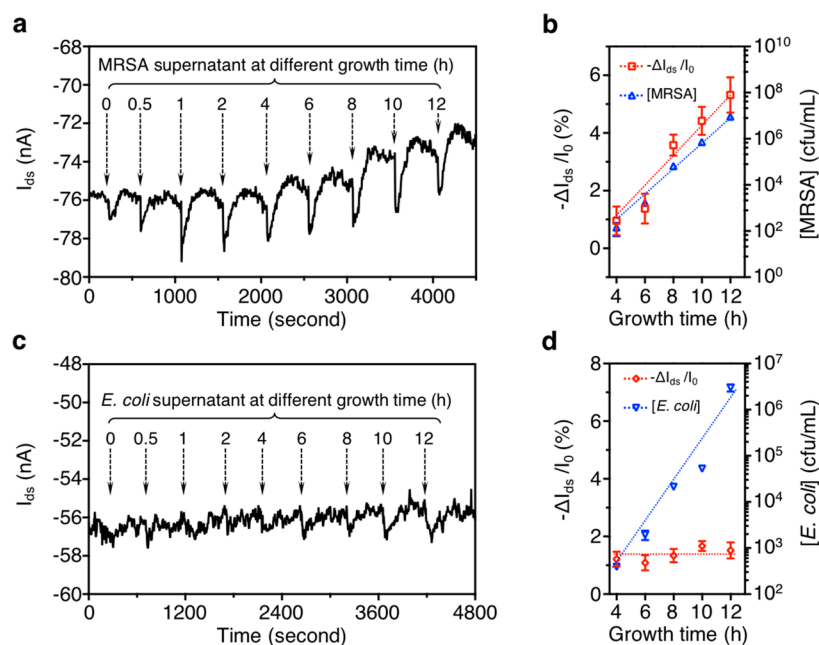


Figure 5. Linear correlation between CM-FET measured signals and bacterial concentrations. (a, b) MRSA USA300 (a bacterial strain that secretes hemolytic toxins) and (c, d) *E. coli* DH5 α (a bacterial strain that does not secrete hemolytic toxins) were used to test the correlation between CM-FET signals and bacterial numbers. For each type of bacteria, bacterial culture supernatants were collected at different growth times and then added onto CM-FETs, and the typical I_{ds} -time curves (a, c) were measured. Values of I_{ds} change relative to the basal level ($\Delta I_{ds}/I_0$) were plotted against bacterial growth time and compared with the corresponding bacterial concentrations in the solutions (b, d). Data represent mean \pm SD. In bacterial enumeration, $n = 3$ independent experiments. In the measurements of $\Delta I_{ds}/I_0$, values of mean and SD were derived from five random points on plateaus in (a) and (c).

using the whole-cell-based assay. The results showed that the percentage of hemolysis induced by supernatant I was indeed significantly lower than those induced by supernatants II and III, while no significant difference of hemolysis was observed with supernatants II and III (Figure 4d). In addition, the hemolytic activity measurements using CM-FETs or the whole-cell-based hemolytic assay correlate well, validating the feasibility and fidelity of CM-FETs as a sensor to measure the total hemolytic activity of complex biological samples (Figure S4).

Correlation of CM-FET Signals with Bacterial Numbers. Finally, we verified the correlation of CM-FET detection signal of hemolytic proteins secreted by pathogens with pathogen numbers in the sample solution. The hypothesis is that through such correlation we can rapidly and accurately determine bacterial numbers (CFU/mL) and types (hemolytic vs nonhemolytic) in a biological fluid by measuring the hemolytic toxins secreted by the bacteria rather than using the traditional agar plate-based culturing method to count bacterial colonies. To test this hypothesis, MRSA USA300 strain was chosen as a model pathogen. To determine the sensitivity of the detection, MRSA bacteria were cultured starting from a low concentration of approximately 1 CFU/mL and the supernatants were collected at various time points of growth for CM-FET measurements (Figure 5a). In the study, ΔI_{ds} remained at the basal level for supernatants collected at no more than 2 h of growth but increased stepwisely for those with longer time of culture, indicating a gradual increase of hemolytic activity as the culture time increased. The measured CM-FET signals were then correlated to the corresponding bacterial concentrations. As shown in Figure 5b, the readout of supernatant from a 4 h culture corresponded to a bacterial concentration of $(1.43 \pm 0.83) \times 10^2$ CFU/mL, which

represented a detection limit of the CM-FET sensor. Moreover, when the plot of $-\Delta I_{ds}/I_0$ was compared to the linear fitting of logarithms of MRSA concentrations, the difference between the slopes of the two curves was insignificant, suggesting a linear correlation between the CM-FET measured signals and the corresponding bacterial concentrations (Table S6). To further confirm such correlation, we performed the same measurements with the culture supernatants of nonhemolytic *Escherichia coli* (*E. coli*) bacteria (Figure 5c,d). CM-FETs showed no response to the bacterial supernatant samples collected at various time points of growth, despite a pronounced increase of the bacterial concentration with culture times. The lack of response to *E. coli* supernatants as opposed to MRSA supernatants confirmed the selectivity of CM-FET toward bacteria that secrete hemolytic proteins. Overall, this experiment demonstrated the potential of using CM-FET for direct, rapid, and sensitive detection of hemolytic pathogens.

CONCLUSIONS

By coating natural RBC membranes onto carbon-nanotube-based FETs, we made a biomimetic nanosensor for amperometric detection of membrane-active biological compounds. Through a fusion process, the cell membranes spontaneously formed a bilayer coating that intimately interfaces with the FETs. In this design, the RBC membranes function as a biological substrate that simulates the natural cells to interact selectively with PFTs. Meanwhile, the FETs serve as an ultrasensitive transducer that responds to the changes in the charge distribution around the FET surface upon toxin absorption. Together, the CM-FETs were capable of rapidly and sensitively detecting a series of PFTs. When applied to analyze the MRSA bacterial culture supernatant, the CM-FET

device responded selectively to membrane-active toxins regardless of their structural and chemical characteristics, therefore demonstrating a function-based detection of membrane active moieties. We further introduced Hl α of known concentrations as an internal reference to overcome the device batch variations. As a result, the CM-FETs were able to provide quantitative measurements of bacterial supernatants in correlation with their overall hemolytic activities as well as the actual bacterial concentrations in the solutions. CM-FETs provide a fast and accurate readout of “severity”, as illustrated by quantitative measurements of hemolytic activity in this study. Such a capability made the CM-FET an attractive device for direct, rapid, and sensitive detection of live pathogens without involving traditional colony-counting methods. The CM-FET can be combined with existing differentiation technologies for further identification of specific toxins or pathogens.

The CM-FET developed here distinguishes itself by the direct use of cell membranes that act as the biological substrate not only to harness specific biological functions but also to interface with FET transducers for highly sensitive readout. As a proof-of-concept study, we selected hemolytic activity as a specific function to evaluate the design and usage of the CM-FET. Notably, as the bacteria harness a diverse range of PFTs with different characteristics for pathogenesis, toward broader applications, the correlation between the hemolytic activity and the sensor readout needs to be established based on the specific bacterial strain. In addition, parameters such as species and blood groups are known to influence toxin-binding ability and pore-forming mechanisms.^{34,35} Therefore, membranes can be further screened to improve on CM-FET sensitivity. As plasma membranes can be derived from a variety of cell types such as platelets, macrophages, cancer cells, and bacterial cells, the CM-FET can thus be constructed with these membranes and a similar working principle can be applied to detect and measure a variety of biological functions and events specific to the corresponding cell types. Meanwhile, the cell membrane can be coated onto a wide range of materials with various structures including nanoparticles,^{15–17} nanofibers,²⁴ and autonomous nanomachines,^{36,37} suggesting the versatility and potential of cell membranes to interface with various transducer platforms. Overall, the CM-FET holds promise as a function-based detection platform for sensitive and quantitative measurements of bioactive molecules and agents.

MATERIALS AND METHODS

Fabrication of Carbon-Nanotube-Based Field Effect Transistors. To fabricate the FETs, a 4 in. Si wafer with a 100 nm thermal oxide layer (SiO₂) was used as the substrate. The wafer was soaked in piranha solution (H₂O₂/H₂SO₄ = 1:3, volume ratio) overnight to remove organic contaminants and to hydroxylate the surface. Subsequently, the wafer was rinsed with DI water and blow-dried with N₂, followed by annealing at 180 °C on a hot plate for 10 min to remove the residue moisture. The electrodes were patterned with a photoresist lift-off technique. Specifically, to pattern the electrode layout, the wafer surface was first spin-coated with an adhesion promoter (80/20 primer, MicroChem) followed by spin coating of a negative photoresist (4000 rpm for 60 s, NR9-3000py, Futurrex). Photoresist soft bake was carried out on a hot plate at 150 °C for 1 min. Exposure was done *via* an L-line mask aligner (SussMicrotec MA6) with 220 mJ dose. Post-exposure annealing at 100 °C for 1 min was conducted to complete the photoreaction initiated under exposure. The exposed sample was then immersed in a tetramethylammonium hydroxide developer (RD6, Futurrex) to be fully developed. For metalization, the sample surface was first cleaned by

oxygen plasma (Trion dry etcher, 50 W, 50 sccm O₂, 50 mTorr, 30 s), followed by deposition of 10 nm of Cr and 100 nm of Au with an electron beam evaporator (Temescal BJD 1800). Lastly, the sample was soaked in acetone to lift off the photoresist and the metal deposited on its surface. The sample was cleaned by rinsing with acetone, isopropyl alcohol (IPA), and DI water and blow-dried with N₂.

Semiconducting single-walled carbon nanotube solution (ISO-Nanotubes-S, NanoIntegris Technologies Inc.) was used to deposit carbon nanotubes onto the surface of the prepared interdigitated electrodes with a spray-coating method. The edge of the SiO₂/Si wafer was covered with a polyimide shadow mask to avoid shorting between the bottom silicon and the top carbon nanotube film. Then the wafer was placed on a hot plate at 180 °C to remove the solvent. A commercial spray gun (model SB-84 from Master Airbrush) was fixed on the top of the wafer with a distance of 12 cm, and the airbrush pressure was around 30 psi. To avoid the merging of sprayed solution, the carbon nanotube solution was sprayed with a duty cycle of 20% (5 s for each cycle: 1 s for spray and 4 s for solvent evaporation). The spray coating took 10 cycles to deposit the carbon nanotube layer. After deposition, the wafer was kept on the hot plate at 180 °C for 3 min to remove any residual solvent. Then the wafer was rinsed with DI water to remove the surface ionic surfactants and blow-dried.

Fabrication of Cell-Membrane-Coated FETs. The red blood cell membranes were derived from human whole blood (Zen-Bio Inc.) based on a previously published protocol.¹⁵ Specifically, the whole blood was first washed with 1× phosphate-buffered saline (PBS, Corning) containing 1 mM ethylenediaminetetraacetic acid (EDTA, Sigma-Aldrich) three times to remove the serum and buffy coat. RBC pellets were then resuspended with 0.25× PBS for a hypotonic treatment and placed on ice for 20 min. Released hemoglobin was then removed with centrifugation (8000g for 3 min). The hypotonic treatment was repeated five times. Purified RBC membranes were finally resuspended in 1× PBS containing 0.2 mM EDTA and stored in a –80 °C refrigerator for future use. To coat the RBC membranes onto the FETs, the RBC membranes were first washed with 1× PBS and then sonicated with a bath sonicator (100 W, FS30D, Fisher Scientific) for 5 min. The resulting solution containing RBC vesicles was adjusted to a membrane protein concentration of 1 mg mL⁻¹ and added directly onto the top of the cleaned FETs. The samples were incubated at 37 °C for 1 h followed by rinsing with 1× PBS three times. To prepare the cholesterol-enriched RBC membrane coating, 2 μ L of cholesterol in chloroform (50 mg mL⁻¹, Fisher Scientific) was first added to 100 μ L of PBS solution and mixed well through gentle shaking. Then 50 μ L of the solution was directly added on top of the FETs in place of PBS and incubated for another 10 min at 37 °C. Bovine serum albumin (BSA, Sigma-Aldrich) solutions at concentrations of 0.1 mg mL⁻¹ were then incubated with the CM-FETs for 30 min at room temperature.

Characterization of the CM-FETs. For the vesicle fusion study, RBC vesicles were fluorescently labeled with DiD (ThermoFisher, excitation/emission = 647/667 nm) into the cell membrane and calcein (Sigma-Aldrich, excitation/emission = 495/519 nm) into the aqueous core. Specifically, DiD was first mixed with RBC ghost at a mass ratio of 1:1000 (DiD:protein content of RBC ghost), and the excess dyes were removed through centrifugation at 8000g three times. The purified ghost at a protein concentration of 1 mg mL⁻¹ was then mixed with calcein solutions (2 mg mL⁻¹) at a volume ratio of 1:1 and sonicated by bath sonication to make RBC vesicles. The excess calcein was removed by a G-25 Superdex column (GE Healthcare Life Sciences). Before and after adding the dual-dye-labeled RBC vesicles onto the FETs, the fluorescence spectra of both calcein and DiD were measured by a microplate reader.

For the FRAP study, RBC vesicles labeled with DiD were used to prepare the CM-FETs following the same procedure as described above. After cell membrane coating, the FRAP study was conducted by using a Leica SPS microscope. A random region of interest between two electrodes was selected and photobleached by a high power density of a 663 nm laser using the zoom-in mode. The fluorescence intensity recovery after photobleaching was monitored.

Images at different time points were derived from videos, while the diffusion coefficient (D) was calculated by using the function $D = 0.88r^2/(4t_{1/2})$ (r , radius of photobleaching area; $t_{1/2}$, time needed to reach half-maximum fluorescence recovery).²⁵

Electronic Properties of the CM-FETs. The FET was placed on the stage of a probe station (1160 series, Signatone). A 30 μL amount of PBS was added on top of the FET, and then three electrodes were placed, namely, the source (S), drain (D), and Ag/AgCl reference (R) electrodes. Both the input voltage and output current were controlled by a source meter (B2912A, Keysight). All of the experiments were conducted in ambient environment. The characterization was conducted at the probe station by measuring the $I_{\text{ds}}-V_{\text{g}}$ (drain-source current versus gate voltage) curve under different V_{ds} (drain-source voltage) for the CM-FET. V_{g} was relative to the source. Various curves were obtained by varying the V_{g} from -0.6 to 0 V. The I_{ds} was recorded while changing the V_{ds} from -0.6 V to -0.1 V with a step size of 0.1 V. For the $I_{\text{ds}}-t$ curve, we compared the I_{ds} change of uncoated FET and CM-FET with complete membrane coating as a function of time. The V_{g} was 0 V and the V_{ds} was -0.3 V. After incubating the device with RBC membrane vesicles for 1 h at 37 °C, the extra membrane vesicles were removed by multiple PBS washings before I_{ds} was measured.

Toxin Detection Study with the CM-FETs. Stock solutions of mellitin (Sigma-Aldrich), Hl α (Sigma-Aldrich), and SLO (Bio-Rad) were prepared by dissolving the toxin dry powders with $1\times$ PBS to a final concentration of 7.0×10^{-7} , 3.0×10^{-5} , and 1.4×10^{-5} M, respectively. Then 10-fold serial dilutions were made from the stock solutions for the detection study. In the study, BSA was used to block nonspecific binding sites prior to the measurements. Toxin solutions were added ($1.2\ \mu\text{L}$ each addition) to the CM-FETs from low to high concentrations. At each concentration, I_{ds} was measured as a function of time, and $\Delta I_{\text{ds}}/I_0$ (%) was defined as $(I_{\text{ds}} - I_0)/I_0 \times 100$ (I_0 is the initial drain-source current, and I_{ds} is the current after adding the toxin).

Bacterial Culture. Methicillin-resistant *Staphylococcus aureus* (USA300) was purchased from American Type Culture Collection (ATCC). The bacterial stock was first cultured on tryptic soy broth agar (TSB, Becton, Dickinson and Company) at 37 °C overnight. Then a single colony was selected and inoculated into 5 mL of TSB medium in culturing tubes (VWR) under shaking at 37 °C for 12 h. Then the bacterial culture in the tubes was transferred to a 200 mL culturing flask (Fisherbrand) and cultured for another 48 h. For batch A supernatant, we harvested 4 mL of the culture supernatant after 6 h of incubation (supernatant I) and 48 h of incubation (supernatant II), respectively. For batch B supernatant, we harvested 4 mL of the culture supernatant after 36 h of incubation (supernatant III). Bacteria were enumerated by measuring the optical density (OD) at 600 nm ($\text{OD}_{600\text{ nm}}$ of $1 = 1\times 10^8$ bacteria mL^{-1}). Then the supernatant was harvested with centrifugation at $5000g$ for 5 min and stored at -80 °C for future use.

Hemolysis Quantification with the CM-FETs. Serial 10 times dilution of Hl α solution (Sigma-Aldrich, 3.03×10^{-5} M, stock concentration) and MRSA culture supernatant were made. In the study, BSA was used to block nonspecific binding sites prior to the measurements. First, we alternately added Hl α and MRSA supernatant from low to high concentrations, and I_{ds} change was recorded as a function of time. The V_{ds} for each device was set at -0.3 V. Second, the I_{ds} change (ΔI_{ds}) corresponding to Hl α or MRSA supernatant was extracted; then the accumulated ΔI_{ds} divided by I_0 ($\Delta I_{\text{ds}}/I_0$, I_0 is the initial current between the drain and source) was plotted against the dilution factors of MRSA supernatant. Third, for the data fitting, two linear curves corresponding to Hl α (red solid line) and MRSA supernatant (blue solid line) were generated through linear regression; then a linear regression fitting with slope constrained to equal the value of the Hl α was applied for the MRSA supernatant (red dashed line). The F test was applied for testing the difference of the two linear fitting curves of the MRSA supernatant (blue solid line, without constrained slope; red dashed line, with constrained slope) to evaluate whether there is statistical significance (significance level was set at 0.05). Fourthly, the distance

between the two parallel linear curves (red solid line for Hl α and red dashed line for MRSA supernatant) was calculated (denoted ΔX). The actual amount of hemolytic toxins in a supernatant sample is unknown, but the concentration of Hl α as an internal reference is well-defined. Therefore, the distance between the two parallel linear curves, ΔX , will thus be able to quantitatively describe the hemolytic activity of a given MRSA supernatant at the equivalence of the hemolytic activity of corresponding Hl α . Lastly, a conventional hemolytic assay using 5% packed RBCs was used to evaluate the hemolytic activity of the MRSA supernatants. Human packed RBCs (Zen-Bio, Inc.) were first diluted in PBS at a volume ratio of $1:20$ (whole blood:PBS) to get a 5% RBC suspension, which was later washed by PBS six times to remove the possible released hemoglobin from the RBCs at $800g$ for 3 min each time.

Correlation of CM-FET Signal with Bacterial Concentrations. MRSA bacteria (USA 300, ATCC) were first inoculated onto a tryptic soy broth (Becton, Dickinson and Company) agar plate and incubated at 37 °C overnight. Following the incubation, a single colony of MRSA bacteria was selected and inoculated into 5 mL of fresh TSB medium. The medium was shaken for 12 h at 37 °C until an optical density at 600 nm (OD_{600}) value of 1.0 (equivalent to 1×10^8 cells/mL) was achieved. The bacteria were then added to 200 mL of fresh TSB medium to a bacterial concentration of 1 colony formation unit (CFU)/mL, followed by culturing at 37 °C with gentle shaking. At $0, 0.5, 1, 2, 4, 6, 8, 10, 12, 14,$ and 24 h of the culture, 1.3 mL of the culture medium was taken. The medium (1 mL) was spun at $4000g$ to remove the bacteria, and the supernatant was collected for the measurement of hemolytic activity with CM-FET. Meanwhile, the remaining medium (0.3 mL) was serially diluted. MRSA bacteria were enumerated by counting bacterial colonies on agar plates and adjusted for dilutions. Studies with *Escherichia coli* (*E. coli*, DHS α competent strain, ATCC) bacteria were performed with the same procedure, except that lysogeny broth agar plates and medium were used for the bacterial culture.

ASSOCIATED CONTENT

Supporting Information

The Supporting Information is available free of charge on the ACS Publications website at DOI: 10.1021/acsnano.9b00911.

Figures of SEM characterization of an uncoated FET device; CM-FET sensing specificity test; I_{ds} of MRSA culture supernatant samples; validation of CM-FET measurement using conventional hemolytic assay; Tables of procedures of using CM-FET to measure toxin hemolytic activity; MRSA culture supernatant samples; list of Hl α concentrations and supernatant dilution factors; goodness of I_{ds} linear fitting; correlation of CM-FET responses between supernatant and Hl α samples; correlation of CM-FET signals with bacterial numbers (PDF)

AUTHOR INFORMATION

Corresponding Authors

*E-mail: shengxu@ucsd.edu.

*E-mail: zhang@ucsd.edu.

ORCID

Liangfang Zhang: 0000-0003-0637-0654

Author Contributions

[†]H. Gong, F. Chen, Z. Huang, and Y. Gu contributed equally.

Notes

The authors declare no competing financial interest.

ACKNOWLEDGMENTS

This project was supported by the Defense Threat Reduction Agency Joint Science and Technology Office for Chemical and

Biological Defense (Grant Numbers HDTRA1-14-1-0064 and HDTRA1-16-1-0013).

REFERENCES

- (1) Kosaka, P. M.; Pini, V.; Ruz, J. J.; da Silva, R. A.; Gonzalez, M. U.; Ramos, D.; Calleja, M.; Tamayo, J. Detection of Cancer Biomarkers in Serum Using a Hybrid Mechanical and Optoplasmonic Nanosensor. *Nat. Nanotechnol.* **2014**, *9*, 1047–1053.
- (2) Rana, S.; Le, N. D. B.; Mout, R.; Saha, K.; Tonga, G. Y.; Bain, R. E. S.; Miranda, O. R.; Rotello, C. M.; Rotello, V. M. A Multichannel Nanosensor for Instantaneous Readout of Cancer Drug Mechanisms. *Nat. Nanotechnol.* **2015**, *10*, 65–69.
- (3) Park, K.; Kuo, Y.; Shvadchak, V.; Ingargiola, A.; Dai, X.; Hsiung, L.; Kim, W.; Zhou, H.; Zou, P.; Levine, A. J.; Li, J.; Weiss, S., Membrane Insertion of—and Membrane Potential Sensing by—Semiconductor Voltage Nanosensors: Feasibility Demonstration. *Sci. Adv.* **2018**, *4*, e1601453.
- (4) Kim, S. J.; Choi, S. J.; Jang, J. S.; Cho, H. J.; Kima, I. D. Innovative Nanosensor for Disease Diagnosis. *Acc. Chem. Res.* **2017**, *50*, 1587–1596.
- (5) Courbet, A.; Endy, D.; Renard, E.; Molina, F.; Bonnet, J. Detection of Pathological Biomarkers in Human Clinical Samples via Amplifying Genetic Switches and Logic Gates. *Sci. Transl. Med.* **2015**, *7*, 289ra83.
- (6) Vishinkin, R.; Haick, H. Nanoscale Sensor Technologies for Disease Detection via Volatolomics. *Small* **2015**, *11*, 6142–6164.
- (7) Wolfrum, B.; Katelhon, E.; Yakushenko, A.; Krause, K. J.; Adly, N.; Huske, M.; Rinklin, P. Nanoscale Electrochemical Sensor Arrays: Redox Cycling Amplification in Dual-Electrode Systems. *Acc. Chem. Res.* **2016**, *49*, 2031–2040.
- (8) Wang, Y.; Duncan, T. V. Nanoscale Sensors for Assuring the Safety of Food Products. *Curr. Opin. Biotechnol.* **2017**, *44*, 74–86.
- (9) Stern, E.; Vacic, A.; Rajan, N. K.; Criscione, J. M.; Park, J.; Ilic, B. R.; Mooney, D. J.; Reed, M. A.; Fahmy, T. M. Label-Free Biomarker Detection from Whole Blood. *Nat. Nanotechnol.* **2010**, *5*, 138–142.
- (10) Sorgenfrei, S.; Chiu, C. Y.; Gonzalez, R. L.; Yu, Y. J.; Kim, P.; Nuckolls, C.; Shepard, K. L. Label-Free Single-Molecule Detection of DNA-Hybridization Kinetics with a Carbon Nanotube Field-Effect Transistor. *Nat. Nanotechnol.* **2011**, *6*, 125–131.
- (11) Ji, M. B.; Orringer, D. A.; Freudiger, C. W.; Ramkissoon, S.; Liu, X. H.; Lau, D.; Golby, A. J.; Norton, I.; Hayashi, M.; Agar, N. Y. R.; Young, G. S.; Spino, C.; Santagata, S.; Camelo-Piragua, S.; Ligon, K. L.; Sagher, O.; Xie, X. S. Rapid, Label-Free Detection of Brain Tumors with Stimulated Raman Scattering Microscopy. *Sci. Transl. Med.* **2013**, *5*, 201ra119.
- (12) Kobayashi, H.; Lei, C.; Wu, Y.; Mao, A. L.; Jiang, Y. Y.; Guo, B. S.; Ozeki, Y.; Goda, K. Label-Free Detection of Cellular Drug Responses by High-Throughput Bright-Field Imaging and Machine Learning. *Sci. Rep.* **2017**, *7*, 12454 DOI: 10.1038/s41598-017-12378-4.
- (13) Olsen, E. V.; Pathirana, S.; Samoylov, A.; Barbaree, J.; Chin, B.; Neely, W.; Vodyanov, V. Specific and Selective Biosensor for Salmonella and Its Detection in the Environment. *J. Microbiol. Methods* **2003**, *53*, 273–285.
- (14) Grieshaber, D.; MacKenzie, R.; Voeroes, J.; Reimhult, E. Electrochemical Biosensors—Sensor Principles and Architectures. *Sensors* **2008**, *8*, 1400–1458.
- (15) Hu, C.-M. J.; Zhang, L.; Aryal, S.; Cheung, C.; Fang, R. H.; Zhang, L. Erythrocyte Membrane-Camouflaged Polymeric Nanoparticles as a Biomimetic Delivery Platform. *Proc. Natl. Acad. Sci. U. S. A.* **2011**, *108*, 10980–10985.
- (16) Fang, R. H.; Hu, C.-M. J.; Luk, B. T.; Gao, W.; Copp, J. A.; Tai, Y.; O'Connor, D. E.; Zhang, L. Cancer Cell Membrane-Coated Nanoparticles for Anticancer Vaccination and Drug Delivery. *Nano Lett.* **2014**, *14*, 2181–2188.
- (17) Hu, C. M. J.; Fang, R. H.; Wang, K. C.; Luk, B. T.; Thamphiwatana, S.; Dehaini, D.; Nguyen, P.; Angsantikul, P.; Wen, C. H.; Kroll, A. V.; Carpenter, C.; Ramesh, M.; Qu, V.; Patel, S. H.; Zhu, J.; Shi, W.; Hofman, F. M.; Chen, T. C.; Gao, W.; Zhang, K.; Chien, S.; Zhang, L. Nanoparticle Biointerfacing by Platelet Membrane Cloaking. *Nature* **2015**, *526*, 118–121.
- (18) Hu, C.-M. J.; Fang, R. H.; Copp, J.; Luk, B. T.; Zhang, L. A Biomimetic Nanosponge That Absorbs Pore-Forming Toxins. *Nat. Nanotechnol.* **2013**, *8*, 336–340.
- (19) Fang, R. H.; Luk, B. T.; Hu, C.-M. J.; Zhang, L. Engineered Nanoparticles Mimicking Cell Membranes for Toxin Neutralization. *Adv. Drug Delivery Rev.* **2015**, *90*, 69–80.
- (20) Maehashi, K.; Katsura, T.; Kerman, K.; Takamura, Y.; Matsumoto, K.; Tamiya, E. Label-Free Protein Biosensor Based on Aptamer-Modified Carbon Nanotube Field-Effect Transistors. *Anal. Chem.* **2007**, *79*, 782–787.
- (21) Zhou, X.; Moran-Mirabal, J. M.; Craighead, H. G.; McEuen, P. L. Supported Lipid Bilayer/Carbon Nanotube Hybrids. *Nat. Nanotechnol.* **2007**, *2*, 185–190.
- (22) Xu, D.; Cheng, Q. Surface-Bound Lipid Vesicles Encapsulating Redox Species for Amperometric Biosensing of Pore-Forming Bacterial Toxins. *J. Am. Chem. Soc.* **2002**, *124*, 14314–14315.
- (23) Stenger, D. A.; Gross, G. W.; Keefer, E. W.; Shaffer, K. M.; Andreadis, J. D.; Ma, W.; Pancrazio, J. J. Detection of Physiologically Active Compounds Using Cell-Based Biosensors. *Trends Biotechnol.* **2001**, *19*, 304–309.
- (24) Chen, W.; Zhang, Q.; Luk, B. T.; Fang, R. H.; Liu, Y.; Gao, W.; Zhang, L. Coating Nanofiber Scaffolds with Beta Cell Membrane to Promote Cell Proliferation and Function. *Nanoscale* **2016**, *8*, 10364–10370.
- (25) Kang, M.; Day, C. A.; Kenworthy, A. K.; DiBenedetto, E. Simplified Equation to Extract Diffusion Coefficients from Confocal Frap Data. *Traffic* **2012**, *13*, 1589–1600.
- (26) Bloom, J. A.; Webb, W. Lipid Diffusibility in the Intact Erythrocyte Membrane. *Biophys. J.* **1983**, *42*, 295–305.
- (27) Filippov, A.; Orådd, G.; Lindblom, G. The Effect of Cholesterol on the Lateral Diffusion of Phospholipids in Oriented Bilayers. *Biophys. J.* **2003**, *84*, 3079–3086.
- (28) Avouris, P.; Chen, Z.; Perebeinos, V. Carbon-Based Electronics. *Nat. Nanotechnol.* **2007**, *2*, 605–615.
- (29) Acevedo, B.; Perera, Y.; Ruiz, M.; Rojas, G.; Benitez, J.; Ayala, M.; Gavilondo, J. Development and Validation of a Quantitative Elisa for the Measurement of Psa Concentration. *Clin. Chim. Acta* **2002**, *317*, 55–63.
- (30) Cui, Y.; Wei, Q.; Park, H.; Lieber, C. M. Nanowire Nanosensors for Highly Sensitive and Selective Detection of Biological and Chemical Species. *Science* **2001**, *293*, 1289–1292.
- (31) Gruner, G. Carbon Nanotube Transistors for Biosensing Applications. *Anal. Bioanal. Chem.* **2005**, *384*, 322–335.
- (32) Chen, K.-I.; Li, B.-R.; Chen, Y.-T. Silicon Nanowire Field-Effect Transistor-Based Biosensors for Biomedical Diagnosis and Cellular Recording Investigation. *Nano Today* **2011**, *6*, 131–154.
- (33) Wei, X.; Gao, J.; Wang, F.; Ying, M.; Angsantikul, P.; Kroll, A. V.; Zhou, J.; Gao, W.; Lu, W.; Fang, R. H. *In situ* Capture of Bacterial Toxins for Antivirulence Vaccination. *Adv. Mater.* **2017**, *29*, 1701644.
- (34) Cooling, L. Blood Groups in Infection and Host Susceptibility. *Clin. Microbiol. Rev.* **2015**, *28*, 801–870.
- (35) Los, F. C. O.; Randis, T. M.; Aroian, R. V.; Ratner, A. J. Role of Pore-Forming Toxins in Bacterial Infectious Diseases. *Microbiol. Mol. Biol. Rev.* **2013**, *77*, 173–207.
- (36) Wu, Z.; Li, T.; Li, J.; Gao, W.; Xu, T.; Christianson, C.; Gao, W.; Galarnyk, M.; He, Q.; Zhang, L.; Wang, J. Turning Erythrocytes into Functional Micromotors. *ACS Nano* **2014**, *8*, 12041–12048.
- (37) Wu, Z.; Li, J.; de Ávila, B. E. F.; Li, T.; Gao, W.; He, Q.; Zhang, L.; Wang, J. Water-Powered Cell-Mimicking Janus Micromotor. *Adv. Funct. Mater.* **2015**, *25*, 7497–7501.